拡散テンソルMRIによる大脳皮質・深部灰白質間の線維連絡解析

林　拓也

神経内科
Reprinted from NEUROLOGICAL MEDICINE
Vol. 65 No. 2 Aug. 2006
科学評論社

神経内科，65(2)：161-168，2006

特集 拡散テンソルに基づくMRIの進歩

拡散テンソルMRIによる大脳皮質・深部灰白質間の線維連絡解析*

林 拓也**

Key Words : diffusion tensor, tractography, striatum, thalamus

はじめに

近年の拡散テンソルMRI(DTI)法の撮像・解析技術の進歩により，脳内の拡散移動度の評価およびそれに基づく脳内の巨視的線維連絡性の評価(diffusion-based tractography)が可能になり，ヒト中枢神経疾患の病態や脳内線維連絡性の解明に貢献すると期待されている．本稿では，とくにdiffusion-based tractographyに関した近年の技術進歩と大脳皮質－深部灰白質間の線維連絡解明の応用研究を紹介し，神経内科領域における臨床検査への応用性について考えてみたい．

脳の拡散異方性からDTI，DTIからtractographyへ

Diffusion-based tractographyはそもそも脳内の水分子の拡散運動(diffusion)が空間的に均等(等方性isotropic)でないという特殊な物理的性質のために可能となった技術である．なぜ神経領域で拡散が等方性でない(逆は異方性anisotropicと呼ぶ)のか未解明な部分も多いが，いくつか面白い研究がある．当初神経領域にのみ存在し電気絶縁体として働く髄鞘(ミエリン)が疑われたが，Beaulieuらはダツという鼻の長い魚の嗅球神経および三叉神経(ご存知の通り，前者は無髄神経，後者は有髄神経の束である)の拡散異方性を調べたところ，どちらも同じ程度の異方性であった(すなわち神経線維走行の方向には拡散しやすく，垂直方向には拡散が制限されていたが，その相対比は同程度であった)[1](図1)．また彼らは，(拡散よりも大きな動きである)軸索流を阻害する薬(vinblastine：微小管の機能を抑制する)を用いたり，軸索膜の寄与の少ないヤリイカ巨大神経を使って，軸索流の影響や軸索内長軸方向の蛋白構造物(microtubuleなど)の影響を検討したが，いずれも異方性に寄与しなかった[1]．その後，他の研究者が髄鞘形成前の新生仔ラットや遺伝性髄鞘欠損ラットの脳でも強い異方性を観察したことから，主に軸索膜，次に髄鞘膜が拡散異方性の原因と考えられている(総説[1]参照)．

Diffusion tensor imaging(DTI)法は，motion probing gradient, MPG[1]という傾斜磁場を均等に多方向(最低6方向)で用いることで相対的拡散移動度の空間的特徴をdiffusion tensorとして表現し画像化する方法である[2]．MPGには方向性があり，MPGと同じ方向の拡散運動が大きい部位で信号が低下する．たとえば，左右方向にMPGを

* Connectivity between cerebral cortex and deep gray matter.

** Takuya HAYASHI, M.D., Ph.D.: 国立循環器病センター研究所放射線医学部〔〒565-8565 大阪府吹田市藤白台5-7-1〕; Department of Investigative Radiology, National Cardiovascular Center, Research Institute, Suita, Osaka 565-8565, Japan.

[1] 兼 モントリオール神経研究所脳画像研究部門; Montreal Neurological Institute, Brain Imaging Center, Montreal, USA.

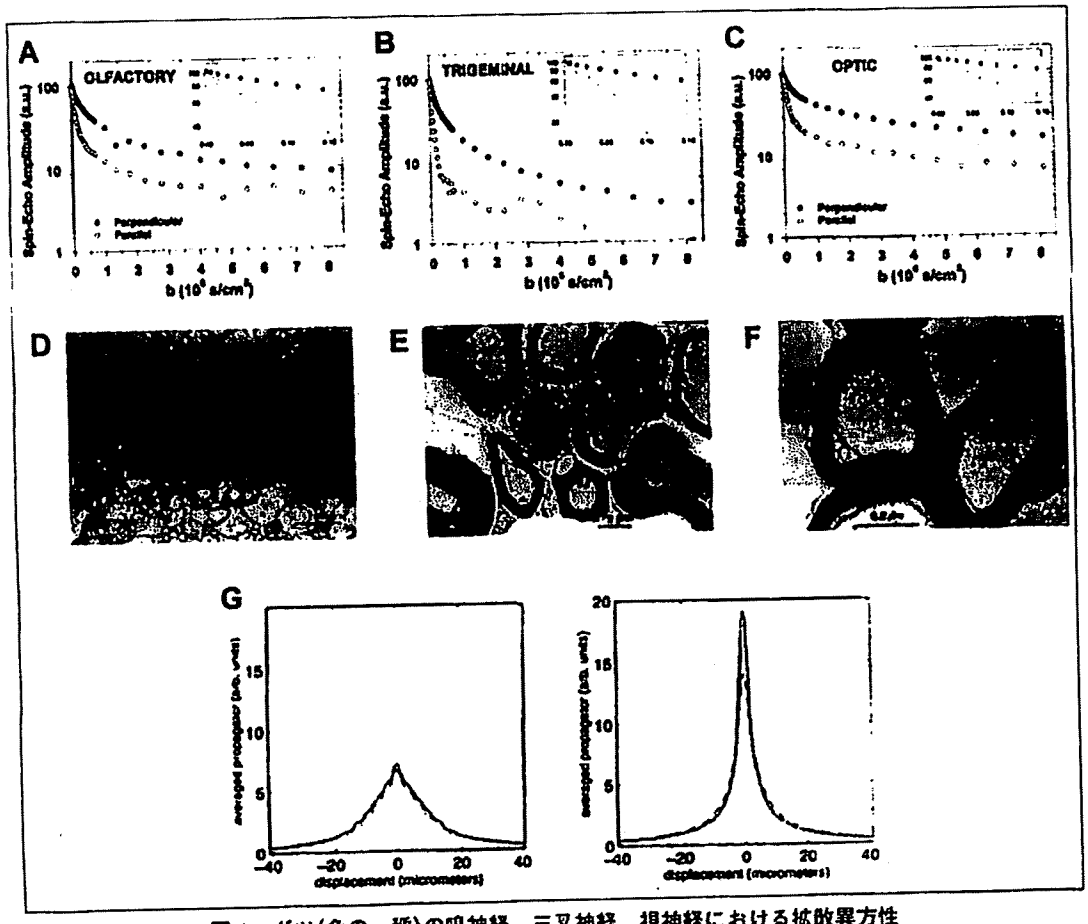

図1　ダツ(魚の一種)の嗅神経，三叉神経，視神経における拡散異方性

嗅神経(A)，三叉神経(B)，視神経(C)における神経線維方向(●)および垂直方向(○)に拡散強調傾斜磁場をかけたときのNMR信号(横軸は傾斜磁場強度の指標b値，縦軸は信号強度を示す)．また，各神経の電顕像をそれぞれD, E, Fに示す．嗅神経は無髄，三叉神経，視神経は有髄神経で，それぞれの神経線維径も違うが垂直方向のNMR信号強度は3神経で同じように低下する．G：実際にこのデータからq-space法によって水分子移動確率分布を計算した結果．3本の神経線維ともに平行方向(右)に比べ垂直方向(左)で明らかに拡散移動が制限されているが，3神経間にはほとんど差がない(実線：嗅神経，破線：三叉神経，点線：視神経)．(文献[1]より改変)

かけると脳梁の部分の信号が低下し，上下方向にかけると内包の部分の信号が低下する．脳内のある一点に注目すると，その部分の水分子がまったく自由に拡散する等方性の状態であれば，原点からの水分子の相対的移動は球になる．一方，方向依存性に拡散が制限される場合(異方性anisotropic)には楕円体になる[‡]．この楕円体または球の形で表される水分子の相対的拡散移動度は数学的概念であるtensorで表現することができ，異なるMPG方向の複数の拡散強調MRIデータから画素毎に計算することができる．この楕円体のもっとも長い軸方向(第一固有ベクトルprincipal eigenvector)は同画素内で支配的に存在する神経線維方向に一致すると考えられる(図2-C)．これを隣の画素同志たどっていくのが神経線維追

* 1965年にStejskal & Tannerが開発した拡散を強調するための傾斜磁場．その後，1986年にLeBihanらが医学領域への応用性を紹介して以後diffusion MRIの医学研究が進んだ．とくに急性期脳梗塞で強い拡散の変化が生じることが発見され，エコープラナーイメージングEPI法と組み合わせて高速撮像が可能となったことで臨床用MRI装置への導入が進んだ．

‡ このtensor modelは非常に単純なモデルで，拡散の均一性と線形性を仮定しているために単純な形状(楕円体)になる．

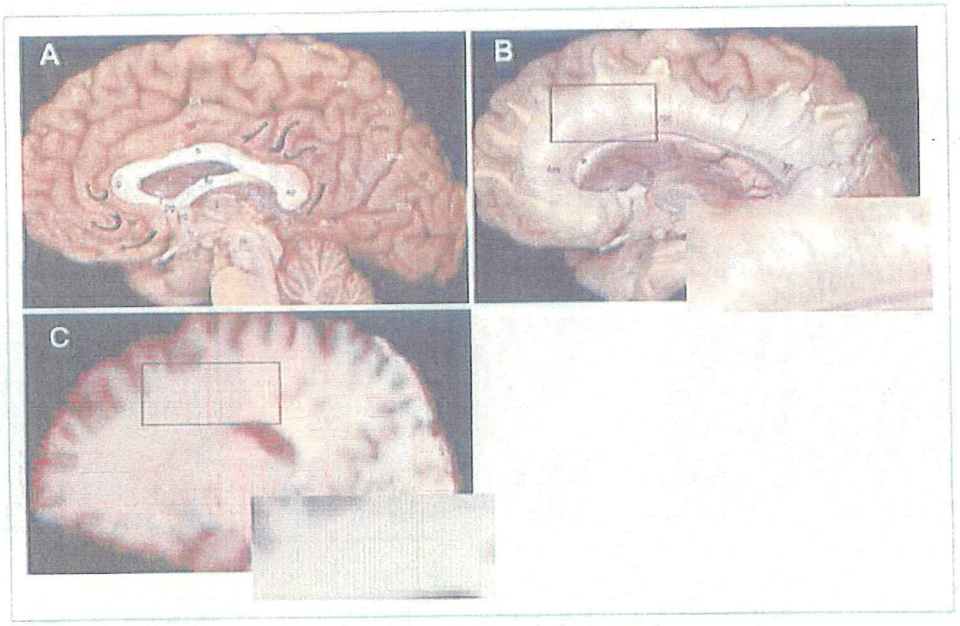

図2　ヒトにおける巨視的神経線維連絡性

A, B：Klingler法による剖検脳の神経線維連絡．右大脳半球内側面(A)から，脳幹部，帯状回皮質，脳梁の内側部が剥離され放線冠(rcc)が露出したところ(B)．黒線の範囲の拡大図を右下に示す．(文献[1]より改変)

C：DTIによる画素ごとのdiffusion tensorの主軸方向．尾状核頭部を通るT1強調矢状断面上にDTI画像解析により得られたtensorの主軸方向を赤線で投射したもの．黒線の範囲の拡大図を右下に示す．隣合う画素の主軸方向があたかも神経線維束に沿うように繋がってみえることがわかる．MPG方向81方向，空間解像度2 mmで収集し，1画素1.2mmの立方体で再構成した画像データからtensorを計算した．

跡法(diffusion-based tractography)であり，この方法の開発には日本人研究者の貢献が大きく，Johns Hopkins大学の森　進教授の方法はこの研究分野を拡大した[3]．

しかし，diffusion-based tractographyはデータ収集・解析法自体に未だ議論が多く，その精度の検証に至っていない．当然，精度高いtensorの推定のために，より方向数の多いMPGによって角度解像度の高い画像収集が望まれている．また，解析の問題として，tracking途中に等方性のtensorに遭遇したとき(すなわち形が球に近いとき)にその主軸方向が推定できず，trackingがそれ以上先に進められなかった．そのため単一方向の線維を支配的に含むような領域(脳梁，錐体路，視放線など)の線維連絡性の評価はできても，線維が交差するような場所や灰白質内の線維連絡性の評価は困難であった．

こうした解析の問題を克服するべく多くの研究が進められており，各画素における各方向の拡散移動をtensorではなく確率分布として表現する方法や，従来のtensor modelに代わり非線形拡散を考慮した方法[5]が提唱されている．前者は，各画素における各方向への拡散移動の確率分布(*pdf*)を，ベイズの定理およびbootstrap法と呼ばれるサンプリング法によって評価し，それに基づいて確率的に線維連絡を評価する(diffusion-weighted probabilistic tractography)[4]．すなわち，従来の方法では画素の間の線維連絡性が繋がるか繋がらないかのバイナリーであったのに対し，このprobabilistic tractographyでは確率と

[5] 前述のように従来のtensor modelは線形性・均一性を仮定していたが，特定の拡散モデルを仮定せず画素内の交差線維を推定するq-ball法[6]，画素内の拡散運動の非線形性を考慮したgeneralized diffusion tensor model法[7]，q-ballと確率的線維連絡追跡法の混合モデル[8]，などが提唱されている．

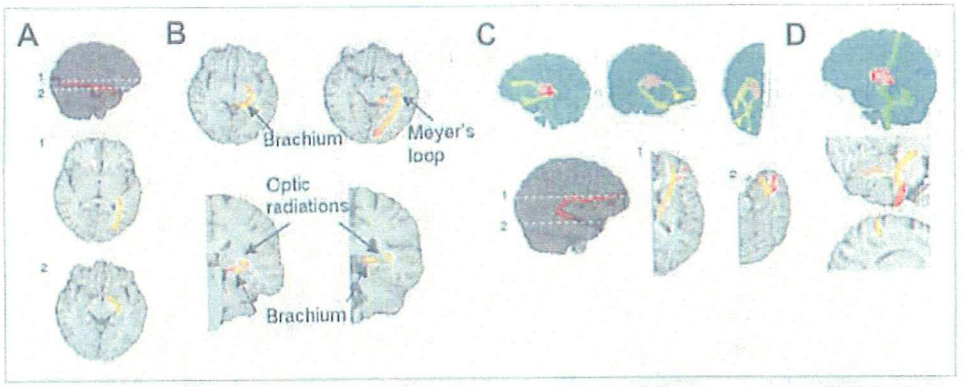

図3　Diffusion-based probabilistic tractographyで観察した視床亜核からの神経線維連絡
A：外側膝状体からの線維連絡をたどったもの．一次視覚野に投射する視放線がみえる．B：同じく外側膝状体から側頭葉内側部を迂回して視覚野に投射する視覚路(Mayer's loop)や上丘腕(Brachium)も観察される．C：視床背内側核からの神経線維連絡．背外側の前頭前野(1)および側頭葉内側部(2)に投射する神経線維を追うことができる．D：視床背外側核からの神経線維連絡．一次運動野および小脳皮質への連絡が観察される．(文献[7]より改変)

して表現したことで線維追跡能を格段に向上させ定量的評価を可能にした．

次項では，この方法により明らかにされてきた大脳皮質と深部灰白質の線維連絡性について述べる．

大脳皮質・深部灰白質間の神経線維連絡

ヒト脳の巨視的な神経線維連絡性の知識はほとんどサル(主にマカク属)脳での神経線維トレーサー(放射能標識アミノ酸，西洋ワサビ過酸化酵素など)によって得られた知見から推定されてきた．ただ，ヒトの巨視的線維連絡性の評価法が今までまったくなかったわけではなく，Klingler法という方法があった[8]．これは神経解剖の教科書でもよくみるもので，剖検脳をまるごとゆっくりと凍結・解凍を繰り返すことで脳組織内の氷の結晶を伸長させ脳内の線維方向に沿った方向にdissectionしやすくするものである．この手法によってヒト脳の脳梁，視放線，錐体路，放線冠，鉤状・弓状束，上・下縦束といった主要な線維束を肉眼的に可視化することができる**(図2-B)．しかし，この手法はdissection自体に技術と経験を要し，その結果も定量的でない[††]．

さて，大脳深部灰白質のうち間脳から発生した「視床」は，脳幹，脊髄，小脳，大脳基底核からの入力を中継し大脳皮質に出力する核である．ヒト剖検脳での組織化学による細胞構築や化学的性質とサル脳での細胞構築・線維連絡性の対応によってかなり視床内核の境界・構造が詳細にわかっている[9]．また，視床内核ごとに大脳皮質との線維連絡性が明確に異なることも知られている．Behrensら[7]は，diffusion-weighted probabilistic tractographyによってヒトの視床を線維連絡性に基づいて分節化することに成功し，この結果が従来知られていた視床内分節化とよく一致した(図4-A)．また同時に，外側膝状体から視覚野へ行く視放線のみならず，視床内側核と前頭前野や側頭葉内側部への線維連絡，視床腹外側核と運動感覚野の線維連絡なども示した(図3-A～D)．また彼らは，この方法によって，脳画像領域で一般に用いられるヒト標準脳空間(モントリオール神経研究所MNIテンプレート)の視床内の各voxelの大脳皮質との連絡性および

** 実際のdissectionの様子をビデオでみることができる(アメリカ脳神経外科学会のwebsite：http://www.aans.org/education/journal/neurosurgical/June05/18-6b-4.pdf内に教育用ビデオのリンクがある)．

†† その他，Nauta法のように損傷脳の剖検脳を用いて，変性した軸索を染色・検索することで損傷部位との線維連絡性を調べる方法や，カルボシアニン色素による剖検脳での線維連絡性評価もあるが，観察機会が限られたり，短い距離の線維連絡しか評価できない．

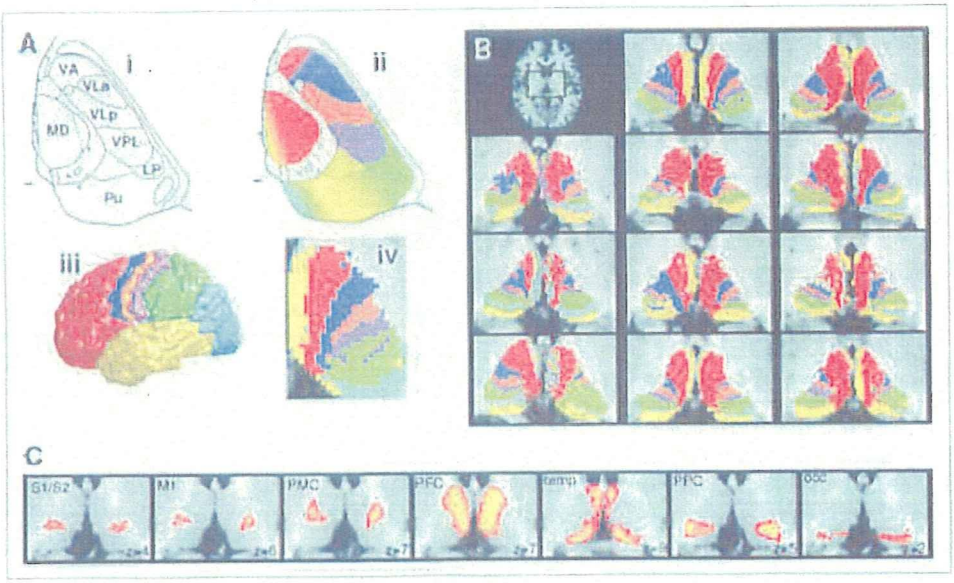

図4　Diffusion-based probabilistic tractographyによる線維連絡性に基づいた視床内の分離
A：視床内の各画素を皮質区分(との線維連絡性に基づいて区分したもの．前検脳による結果(i, ii)と相同的な分離構造が観察される．B：個人ごとの視床内分離．C：複数の個人の脳から得られた標準空間内におけるtractographyに基づいた視床区分アトラス．S1/S2：一次・二次感覚野，M1：一次運動野，PMC：前運動野，PFC：前頭前野，temp：側頭葉，PPC：後部頭頂葉，OCC：後頭葉．(文献[4]より改変)

それに基づく視床内核のアトラスを作成した(図4-C)．しかし，最近のサル脳の研究で皮質から視床への逆行性線維が発見され注目されている[8]が，残念ながら現存のdiffusion-based tractographyで線維連絡の方向性(神経細胞→軸索末端または軸索末端→神経細胞)はわからない．

大脳深部灰白質のうち大脳皮質と同じく終脳から発生した「大脳基底核」は，運動，認知，感情，報酬，学習，言語などさまざまな脳機能に関連する重要な脳部位である．そのうち線条体は神経内科領域でもParkinson病やHuntington病をはじめとする多くの変性疾患の病態に関与する馴染みある部位である．線条体は被殻と尾状核に分かれるが，発生学的に同じ構造物であり，細胞構築も比較的均一で組織化学による染色でも明確な線条体内の境界は認められない．損傷・疾患脳の観察で，特定の神経脱落症状が出現する場合もあるが，何も症状を示さないこともあり機能の局在化が難しい．そのためか古くからサル脳によるトレーサー研究で大脳皮質との連絡性に基づいた線条体内のマッピングを行った研究が多く，それらの観察から大脳皮質－大脳基底核－視床－大脳皮質からなる神経回路(ループ)に関連したモデルも提唱された．

そのうちAlexanderら[9]が提唱したparallel loop modelがもっとも有名なものである．これは大脳皮質，とくに前頭葉皮質の異なる部位からの線維連絡が線条体・視床を(多シナプス性に)経由して再び大脳皮質の同じ部位に投射するとする考え方で，当時はあたかもループ間の情報交換がなく独立して並列処理されているようなものと捉えられ大きな議論が起こった．近年は，上述したようにサル脳での大脳皮質から視床への逆行性線維や，視床から線条体への逆行性線維の発見など[8]により，お互いのループは，従来考えられてきたような閉鎖的(closed loop)ではなく開放的(open loop)であるという考えに変わってきている．Alexanderがparallel loop modelを提唱した当時，心理学や人工知能の分野でも並列分散処理モデル(parallel distributed processing model[10])が注目されはじめたが，このモデルも並列処理間は独立でなく「ゆるやかに制約し合いながら」同時処理するという考えが基本にある[11]．

小生は線条体と大脳皮質との間の線維連絡性に

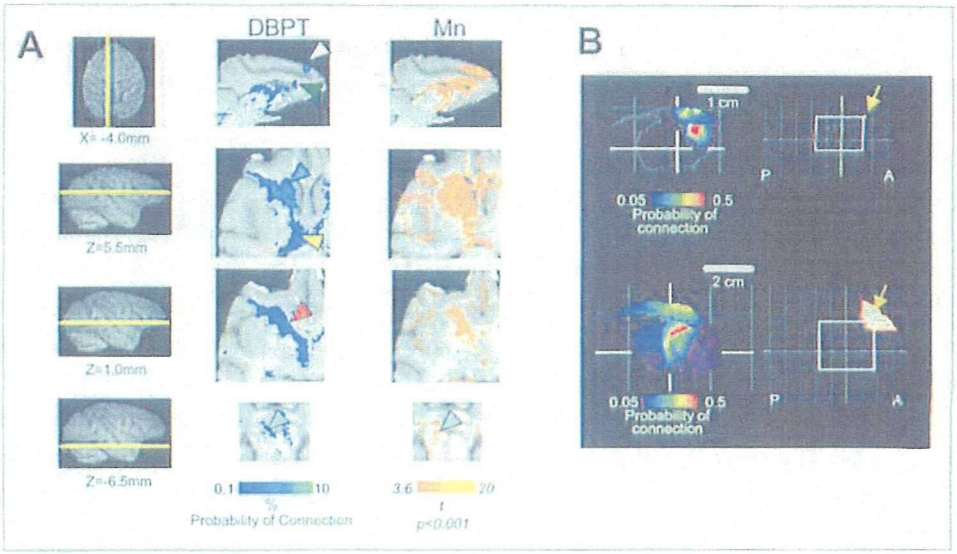

図5　Brodmann 9野（BA9）からの線維連絡性

A：サル脳における線維連絡．Diffusion-based probabilistic tractography（DBPT）によって左BA9からの線維連絡が脳梁，尾状核，被殻，視床内側部，中脳黒質へ伸びていた．これら結果はマンガン（Mn）による神経線維追跡法の結果とよく一致していた．

B：ヒト・サルにおけるBA9の線維連絡性の線条体内分布．最大線維連絡性および線条体の輪郭を矢状面に投射して表示した結果．両種とも尾状核頭部，被殻頭側に投射している．右にBA9の領域を示す．

注目している．サルの大脳皮質前頭葉のBrodmann 9野は，複数の研究者（Brodmann, Vogt, Walkerら）により再現性高く同定されている皮質領域であるが，この部位からprobabilistic tractographyを行うことで尾状核，被殻，視床内側部，中脳腹側，脳梁など複数の場所で，同一個体におけるマンガン（Mn）を用いた神経線維追跡法と非常によく一致した結果が得られた（図5-A）．マンガンは神経細胞にとり込まれて軸索流により遠位に運ばれるanterograde tracerなので[11]，diffusion-based probabilistic tractographyがBrodmann 9野の神経線維連絡を十分な感度と特異性をもって追跡可能であることを示している．

また，ヒトでもBrodmann 9野の線条体連絡部位が相同的に位置するか調べるため複数のヒト剖検脳から作成されたヒト脳標準空間内Brodmann 9野（population-based BA9）[12]からの線維連絡を評価した結果も，サルと同様にヒトも尾状核・被殻の背吻側部にもっとも強い線維連絡が終始することがわかった（図5-B）．実際に前頭葉を中心とした皮質をサル・ヒト間で相同的に5領域に分けてこれら区画と線条体内の各画素間の線維連絡性を計算すると，ヒト・サルともに皮質線維が線条体内でtopographicalに分布し両種間で類似していた（図6）．

今後の展開と臨床応用

Diffusion-based tractographyによるヒト脳内の線維連絡性の評価は未だ撮像や解析技術の面から進歩が望まれる．高解像度の角度のMPGによる画像収集，画素内の交差性線維の推定モデルの導入などにより，今後より高感度の方法ができてくると思われる．しかし，単一画素内の拡散性がいかに正確に捉えられたとしても，現在の拡散強調MRIの解像度は通常ミリメートルの単位でしか収集できず，単一神経線維の径（マイクロメートル単位）に及ばない．そのため画素内で線維が交差しているのか，折れ曲がった線維が接しているだけなのかの区別は不可能である．そのため交差線維の推定感度が上がるにつれ「線維連続性」に関する情報を別の手法で補うことも

‡‡ この辺りは心理学者・守　一雄氏による解説本[13]がわかりやすく面白い．

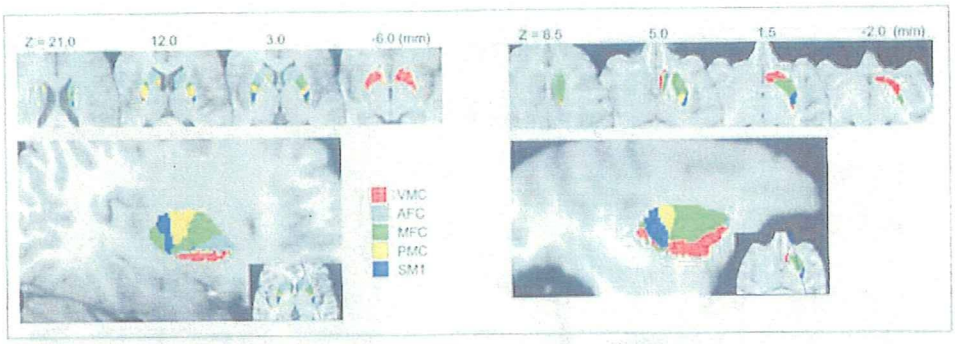

図6　ヒト・サルでの線条体内の皮質線維連絡分布

サル(右)・ヒト(左)において前頭葉を中心とした皮質を5区分に分け，それら皮質と線条体内の各画素間の線維連絡性を算出し，最大線維連絡性を色分けして表示した結果．両種とも，被殻では皮質からの線維がもっとも近い被殻内部にtopographicalに分布していた(closest rule[51])．VMC：帯状回・眼窩前頭皮質，AFC：前頭極，MFC：前頭前野，PMC：前運動野，SM1，傍中心構皮質(一次運動感覚野)．

必要と思われる．また，前述のように「線維の方向性(神経細胞→軸索末端または軸索末端→神経細胞)」の評価はできない．

近年，MRI装置の高磁場(3テスラ)化やマルチコイル化が進み高SN比，短時間で歪みの少ない画像収集がDTI領域でも期待されている．一方，MPGは強力であるほど拡散運動に感度が高いため，より高いb値(MPGの強さの指標)での撮像が望ましいが，その場合，磁場変動の安全性の問題がかかわってくる．とくにq-ball法は角度200方向以上でより高いb値を含めた収集が望まれるため安全面からヒトに応用しにくい．Tractographyの解析モデルと並行した撮像技術開発も望まれる．

DTIをどのように神経内科領域で応用できるか未だ全貌はみえないが，①多くの神経変性疾患が特定の深部灰白質核の変性を伴うこと，②大脳皮質・深部灰白質間の線維連絡性の定量的評価が可能になってきたこと，から少なくとも神経変性疾患の病態研究に応用できると考えられる．しかし，上述のようにこの方法は常に精度・再現性ともに十分な検討が必要である．動物脳で神経線維追跡トレーサーを用いることで「線維連続性」や「線維の方向性」を確認することもその一つの方法であろう．

本稿の一部は厚生労働省科学研究費・こころの健康科学(kokoro-H17-025)の支援を受けた．また，DTIシーケンス開発に尽力いただいた佐藤博司(国循研・先進診断機器開発室)，浦山慎一(京大・高次脳機能研究センター)，MRI撮像・解析に協力いただいた花川　隆，福山秀直(京大・高次脳機能研究センター)，山本明秀，渡部浩司，寺本　昇，飯田秀博(国循研・放医)各氏に深謝する．DTI解析にはオックスフォード大学脳機能MRIセンターの開発したソフトウェア(FSL, http://www.fmrib.ox.ac.uk/fsl/)のdiffusion toolbox (FDT)を使用した(FSLはフリーのソフトウェアで研究用に使用できる)．

文　献

1) Beaulieu C. The basis of anisotropic water diffusion in the nervous system—a technical review. NMR Biomed 2002；15(7-8)：435-55.
2) Basser PJ, Mattiello J, LeBihan D. MR diffusion tensor spectroscopy and imaging. Biophys J 1994；66：259-67.
3) Mori S, Crain BJ, Chacko VP, et al. Three-dimensional tracking of axonal projections in the brain by magnetic resonance imaging. Ann Neurol 1999；45：265-9.
4) Behrens TE, Woolrich MW, Jenkinson M, et al. Characterization and propagation of uncertainty in diffusion-weighted MR imaging. Magn Reson Med 2003；50：1077-88.
5) Klingler J. Erleichterung der makroskopischen Präparation des Gehirns durch den Gefrierprozess.

Schweiz Arch Neurol Psychiatr 1935 ; 36 : 247-56.
6) Morel A, Magnin M, Jeanmonod D. Multiarchitectonic and stereotactic atlas of the human thalamus. J Comp Neurol 1997 ; 387 : 588-630.
7) Behrens TE, Johansen-Berg H, Woolrich MW, et al. Non-invasive mapping of connections between human thalamus and cortex using diffusion imaging. Nat Neurosci 2003 ; 6 : 750-7.
8) Haber S, McFarland NR. The place of the thalamus in frontal cortical-basal ganglia circuits. Neuroscientist 2001 ; 7 : 315-24.
9) Alexander GE, DeLong MR, Strick PL. Parallel organization of functionally segregated circuits linking basal ganglia and cortex. Annu Rev Neurosci 1986 ; 9 : 357-81.
10) Rumelhart DE, McClelland JL, The-PDP-Research-Group. *Parallel distributed processing* : MIT press ; 1986.
11) Sloot WN, Gramsbergen JB. Axonal transport of manganese and its relevance to selective neurotoxicity in the rat basal ganglia. Brain Res 1994 ; 657 (1-2) : 124-32.
12) Rajkowska G, Goldman-Rakic PS. Cytoarchitectonic definition of prefrontal areas in the normal human cortex : II. Variability in locations of areas 9 and 46 and relationship to the Talairach Coordinate System. Cereb Cortex 1995 ; 5 : 323-37.
13) Yasargil MG, Ture U, Yasargil DCH. Surgical anatomy of supratentorial midline lesion. Neurosurgical Focus 2005 ; 18(6b) : E1.
14) Johansen-Berg H, Behrens TE, Sillery E, et al. Functional-anatomical validation and individual variation of diffusion tractography-based segmentation of the human thalamus. Cereb Cortex 2004 ; 15 : 31-9.
15) Kemp JM, Powell TP. The cortico-striate projection in the monkey. Brain 1970 ; 93 : 525-46.

* * *

ELSEVIER

NeuroImage

www.elsevier.com/locate/ynimg
NeuroImage 33 (2006) 1126–1135

Quantitative mapping of basal and vasareactive cerebral blood flow using split-dose ^{123}I-iodoamphetamine and single photon emission computed tomography

Kyeong Min Kim,[a,f] Hiroshi Watabe,[a] Takuya Hayashi,[a] Kohei Hayashida,[b] Tetsuro Katafuchi,[b] Naoyuki Enomoto,[b] Toshiyuki Ogura,[c] Miho Shidahara,[a] Shugo Takikawa,[c] Stefan Eberl,[d] Mayumi Nakazawa,[e] and Hidehiro Iida[a,*]

[a]*Department of Investigative Radiology, National Cardiovascular Center Research Institute, 5-7-1 Fujishiro-dai, Suita City, Osaka, 565-8565, Japan*
[b]*Department of Radiology, National Cardiovascular Center Hospital, Osaka, Japan*
[c]*Department of Neurosurgery, Azabu Neurosurgery Hospital, Sapporo City, Japan*
[d]*Department of Nuclear Medicine, Royal Prince Alfred Hospital, Sydney, Australia*
[e]*Nihon Medi-Physics, Tokyo, Japan*
[f]*Nuclear Medicine Laboratory, Korea Institute of Radiological and Medical Sciences, Seoul, Korea*

Received 17 October 2005; revised 1 March 2006; accepted 25 June 2006
Available online 10 October 2006

A new method has been developed for diffusible tracers, to quantify CBF at rest and after pharmacological stress from a single session of dynamic scans with dual bolus administration of a radiotracer.

The calculation process consisted of three steps, including the procedures of incorporating background radioactivity contaminated from the previous scan. Feasibility of this approach was tested on clinical SPECT studies on 16 subjects. Two sequential SPECT scans, 30 min apart, were carried out on each subject, after each of two split-dose administrations of 111 MBq IMP. Of these, 11 subjects received acetazolamide at 10 min before the second IMP injection. Additional PET scans were also carried out on 6 subjects on a separate day, at rest and after acetazolamide administration. The other 5 subjects were scanned only at rest during the whole study period.

Quantitative CBF obtained by this method was in a good agreement with those determined with PET (y(ml/100 g/min) = 1.07 × (ml/100 g/min) − 1.14, r = 0.94). Vasareactivity was approximately 40% over the whole cerebral area on healthy controls, which was consistent with a literature value. Reproducibility of CBF determined in the rest–rest study was 1.5 ± 5.7%. Noise enhancement of CBF images, particularly the second CBF, was reduced, providing reasonable image quality.

Repeat assessment of quantitative CBF from a single session of scans with split-dose IMP is accurate, and may be applied to clinical research for assessing vascular reactivity in patients with chronic cerebral vascular disease.

Keywords: Split-dose administration; ^{123}I-IMP SPECT; CBF mapping

Introduction

Positron emission tomography (PET) and single photon emission computed tomography (SPECT) are capable of providing physiological functions *in vivo* in a quantitative manner. This is based on mathematical modeling of the kinetic behavior in the body of a tracer that highlights the physiological processes of interest. Two important assumptions are often made, namely, (a) the physiological functions measured are constant over the whole study period, and (b) there is no residual tracer in the body before the tracer administration. These requirements give rise to a crucial restriction in the detection of temporal change of physiological parameters such as cerebral blood flow (CBF). Only a single set of parameters can be determined for a given physiological condition from a series of PET or SPECT measurements. In case of additional assessment at a different physiological condition, an additional scan has to be initiated after decay or excretion of the radioactivity from the body, and the stimulation needs to be applied before the next scan.

One advantage of tracer with a short-lived radioisotope such as ^{15}O in PET is that the radioactivity decays quickly (approximately 2 min half life), which allows a repeat assessment of CBF for several condition within a reasonable interval of typically 10–15 min. However, most PET tracers with longer half-lived radioisotope, such as ^{18}F and ^{11}C, and most SPECT tracers, require background radioactivity compensation, which may be obtained by using the first scan as background or performing an additional image immediately before the second tracer injection. This background subtraction method has been applied to many perfusion studies with SPECT (Hashikawa et al., 1994; Oku et al., 1994; Hattori et al., 1996; Imaizumi et al., 2002), and even to $H_2^{15}O$

* Corresponding author. Fax: +81 6 6835 5429.
E-mail address: iida@ri.ncvc.go.jp (H. Iida).
Available online on ScienceDirect (www.sciencedirect.com).

1053-8119/$ - see front matter © 2006 Elsevier Inc. All rights reserved.
doi:10.1016/j.neuroimage.2006.06.064

PET studies (Chmielowska et al., 1998; Chmielowska et al., 1999). The subtraction method, however, degrades the image quality and quantitative accuracy. A tracer that shows clearance or limited retention in the tissue requires minimizing the scan period for the background not to affect the parameter estimation in the second scan, but this results in the degraded image quality. In turn, a prolongation of the background scan, intended to prevent degrading image quality, causes inconsistency with the parameter estimation due to the time-dependent distribution of the tracer in the next. Clearance of the tracer from tissue is observed not only in the PET study using $H_2^{15}O$ but also in several SPECT studies, such as ^{123}I-iodoamphetamine (IMP) for quantitation of CBF (Iida et al., 1994a,b).

For repeat CBF studies in a single session, we have presented a new mathematical formulation to compensate for the background radioactivity contamination in tissue from the tracer previously administered (Iida et al., 2000; Nishizawa et al., 2003). This allows estimation of "snapshot"-like background radioactivity distribution just before the second tracer scan from the information obtained from whole the previous scan data assuming a compartment model. This background distribution was then built into a model for the parameter estimation using the second tracer data. Based on this formulation, we demonstrated the applicability of this approach to repeat CBF measurement using $H_2^{15}O$ PET in a shorter interval (Watabe et al., 2002).

In this study, we have aimed to make the CBF images of repeat SPECT scan, based on the above formulation, and to evaluate the validity and applicability of this functional mapping method by means of clinical studies performed with SPECT and IMP. Quantitative accuracy of this method was also tested by comparing CBF values with those in $H_2^{15}O$ PET studies.

Materials and methods

Theory

The new mathematical approach, Dual-Table autoradiography (ARG) method was formulated for a cerebral perfusion tracer, which has high trans-capillary extraction to the cerebral tissue with significant clearance. IMP has been chosen in this study. It was assumed that the kinetics of this tracer follows a single-tissue compartment model (Kuhl et al., 1982; Iida et al., 1994a, b). The calculation of CBF at baseline and after the pharmacological stress included three processes as shown in Fig. 1. The first process calculates a CBF (f_1) map from an early image obtained immediately after the first tracer administration based on a previously validated *in vivo* autoradiography technique for IMP, by employing a lookup table procedure (Fig. 1A) (Iida et al., 1994a,b; Iida et al., 1996). The second process estimates a background radioactivity distribution immediately before the next injection of IMP, using the CBF image obtained from the first process (Fig. 1B). This is an inverse procedure of the first process, but estimates the momentary ("snapshot"-like) radioactivity distribution at the time of the second IMP injection. The third process then calculates a CBF (f_2) map after the pharmacological stress from the next early image in addition to the background image generated by the second process (Fig. 1C). For this calculation, the tissue radioactivity concentration was formulated as follows;

$$\int_{T_1}^{T_2} C_i(t)\mathrm{d}t = f_2 \cdot \int_{T_1}^{T_2} C_a(t) c \otimes e^{-\frac{f_2}{V_d} t}\mathrm{d}t + C_i\left(T^{bkg}\right) \cdot \int_{T_1}^{T_2} e^{-\frac{f_2}{V_d}\cdot\left(tzz - T^{bkg}\right)}\mathrm{d}t \quad (1)$$

where $C_i(t)$ is regional tissue radioactivity concentration (cps/g) in the next early image at time t, f_2 CBF (ml/min/g) after the pharmacological stress, V_d distribution volume of the tracer (ml/ml), T_1 and T_2 the scan start and end times for the second scan, respectively, T^{bkg} is the time defined for the background activity before T_1, $C_a(t)$ arterial input function (cps/g), and $\otimes$ convolution integral, respectively. The first-pass extraction fraction is assumed to be unity and independent of time.

The lookup table process therefore includes two tables (see Fig. 2), namely response to the second tracer administration (the first term in the right of Eq. (1)) and the contribution of remaining radioactivity (the second term in the right of Eq. (1)). The second table is scaled by the background counts, $C_i(T^{bkg})$.

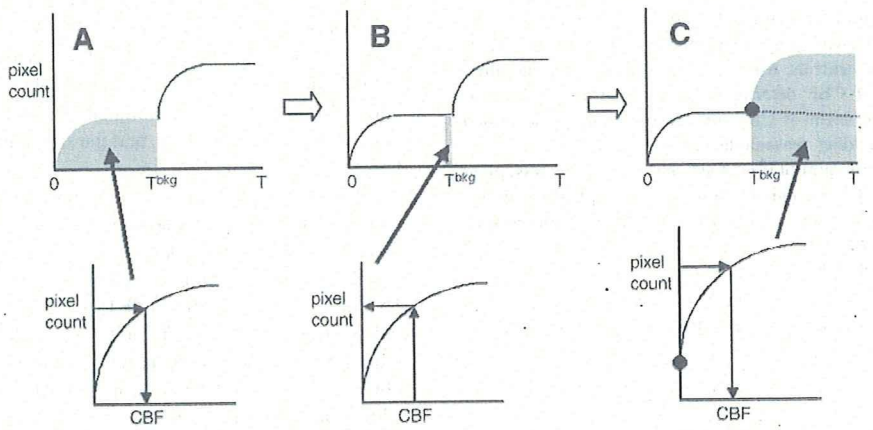

Fig. 1. Mathematical procedure to estimate the first and second CBF maps from a series of SPECT scans following split-dose administration of IMP. The calculation process consists of three steps, namely, (A) calculation of a baseline CBF map from the early image according to the IMP autoradiography, (B) estimation of a transient radioactivity distribution at the end of the scan (or at the time of the next scan initiation) from the CBF map, and (C) calculation of additional CBF map from the second SPECT image. Note that the estimated background distribution is implemented in the model formulation of the second CBF calculation process. Pharmacological stress can be given prior to the second IMP administration in a typical clinical study.

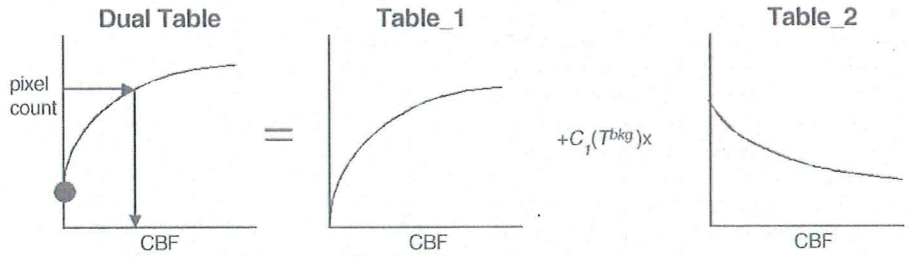

Fig. 2. The procedure to estimate the CBF map from the second SPECT scan. Once a table between CBF and SPECT counts is generated, a lookup table procedure provides a CBF map from pixel counts of the second SPECT image. This table is the sum of two tables corresponding to each term of Eq. (1). The first component corresponds to the response to the newly supplied tracer, and the second table corresponds to the contribution of background activity. Note that the second table is scaled in each pixel by referring the background radioactivity counts at the time of the second scan initiation, which are generated from the previous CBF map.

It is likely that CBF varies during the scan, particularly when pharmacological challenge is given before the end of the first scan. With the definition of a transient weight function, $w(t)$, describing effects of the transient CBF change on the estimated background radioactivity that should be used in the next CBF calculation, the observed tissue concentration, $C_i(T)$, is expressed with $w(t)$ and the transient CBF or $f(t)$ as (Iida et al., 1991);

$$C_i(T) = \int_0^T w(t) \cdot f(t) \mathrm{d}t \tag{2}$$

With assuming a two-compartment model for a constant f during the study and differentiation, $w(t)$ can be approximated by;

$$w(t) \approx \frac{\mathrm{d}C_i(t)}{\mathrm{d}t} \tag{3}$$

Thus the transient weight in the estimated background image is nearly equal to the first derivative of the tissue concentration curve during the previous scan. This suggests that the estimated background distribution for the next scan is predominantly sensitive to flow during the rising period following the bolus injection of IMP, and is only moderately affected by flow after a certain period has elapsed from the previous scan. Thus, minimal effects are expected in the background estimation process, even when pharmacological stress is applied before end of the previous scan.

Subject

Studies were performed on subjects. Subjects were divided into 3 groups. The first group ($n=5$) was consisted of clinical patients with cerebral ischemia, who were assigned to the IMP SPECT studies for clinical diagnosis, and were used to evaluate the reproducibility of the method. In this group, patients were scanned at rest during the whole study period (rest–rest condition). Their age ranged from 51 to 71 years old (mean±SD; 61±9). Four patients suffered from chronic cerebral hemorrhage, and one had an unruptured aneurysm.

The second group consisted of only healthy male volunteers ($n=5$), who had no signs or symptoms of stroke or other ischemic diseases, and were expected to show normal range of CBF values. All subjects belonging to this group were studied at rest during the first scan, but acetazolamide (ACZ) was administrated before the second IMP injection (rest-ACZ condition). Their ages ranged from 27 to 35 (mean±SD; 30±4).

The third group included 6 patients with stenosis or occlusion of extracranial internal carotid artery on unilateral ($n=3$) or bilateral ($n=3$) side. Their age ranged from 71 to 74 years old (mean±SD; 72±1). All patients underwent the IMP SPECT scans at rest and with an acetazolamide challenge, as in the second group, and PET scans following intravenous ^{15}O–water both at rest and after the same dose of acetazolamide, were done 2 days apart from the SPECT study with acetazolamide challenge. The second scan data of one subject among the subjects in this group, were excluded in the data analysis, because of the severe head motion and urination during SPECT acquisition.

All subjects had MRI scans prior to the SPECT study, which has been used for identification of region-of-interest (ROI) and also for generating attenuation maps that have been utilized for corrections of attenuation and scatter in the SPECT reconstruction (see below). All subjects gave written informed consent, and were studied by the protocol approved by the local ethical committee.

SPECT scan

All SPECT studies were carried out following the split-dose administration of IMP. For the first and the second groups, a triple-headed SPECT camera attached with low-energy high-resolution fan-beam collimator (GCA-9300A, Toshiba Medical System, Tokyo, Japan), installed at Azabu Neurosurgery Hospital, was used. And a dual-headed gamma camera attached with low-energy high-resolution fan-beam collimator (ECAM, Siemens Medical System, USA), installed at National Cardiovascular Center Hospital was used for the third group. The size of acquired projection was 64-by-64 pixels, and the energy window selected was 20% on the center of 159 keV for all studies.

In each subject, the split-dose IMP injections (111 MBq each) were separated by an interval of 30 min. The infusion period was 1 min, and was controlled using a constant infusion pump (Terumo, Tokyo, Japan). Two sets of dynamic SPECT scans were initiated at the time of the IMP injection. The duration of each dynamic scan was 30 min for the 1st and 2nd groups and 25 min for the 3rd group, respectively. For both SPECT scans, the detectors were rotated continuously collecting 60 projections over 360° initially every 10 s and, after 5 min, every 2 min for the triple-headed camera, and initially every 2 min and, after 10 min, every 5 min for the dual-headed camera. The acquired projection data

were re-binned to parallel beam projection for further process. Each dynamic projection data with the parallel-beam transformation were summed to a static data for each session, and two sets of images were reconstructed for further image calculation (see below). In the second and third groups, 16 mg/kg (1000 mg maximum) of acetazolamide was administered intravenously at 20 min after the first IMP injection.

Arterial input function was determined in individual studies. Arterial blood was sampled from the radial artery at 15-s intervals during the first 2 min with gradual prolongation thereafter. The whole blood radioactivity concentration was counted using a well counter, and its octanol extraction fraction was also counted as reported previously (Kuhl et al., 1982; Lear et al., 1982; Kurisu et al., 2002).

A uniform cylindrical phantom of 16-cm diameter (axial length of 15 cm) filled with approximately 20 MBq of ^{123}I-solution was scanned following the same scan protocol as for the clinical SPECT studies. The solution was sampled and its radioactivity concentration was counted in the well counter that was used for measuring the arterial blood radioactivity concentration.

PET scan

Six subjects belonging to the third group underwent a series of PET scans within 2-day period from the IMP study. The ECAT Exact47 PET scanner (Siemens-CTI Inc., Knoxville, USA) was used, which provides 47 tomographic slices. The observed spatial resolution of reconstructed image was approximately 7-mm FWHM both in-plane and in axial direction.

After a transmission scan for attenuation correction, a 90-s scan was performed following a bolus injection of ^{15}O-labeled water ($H_2^{15}O$). The functional CBF images were calculated according to the $H_2^{15}O$ autoradiography (ARG) technique (Kanno et al., 1987). The partition coefficient of water was assumed to be 0.80 ml/g, which was meant to minimize effects of tissue heterogeneity (Iida et al., 1988). The arterial input function was determined from the continuously monitored arterial blood time–activity curve including corrections for delay and dispersion (Iida et al., 1986, 1989). The scans were performed twice, the first at rest, and the second at 10 min after administration of the same dose of acetazolamide as in the SPECT study.

SPECT image reconstruction

To generate uniform attenuation map by means of MRI image, both static projections of the first and second sessions were reconstructed without correction of attenuation or scatter, to provide SPECT images for each session, and MRI image of each subject was co-registered to the reconstructed image without attenuation correction, using SPM2 (Welcome Department of Imaging Neuroscience, University College London, London, UK). The co-registered MRI image was converted to an attenuation map, after defining the head contour and assigning a value of uniform attenuation coefficient of 0.167 cm^{-1} into the area inside the head contour (Iida et al., 1998). The uniform attenuation map was used in image reconstruction with corrections of attenuation and scatter. Scatter component in emission projection was corrected by employing a technique of transmission-dependent convolution subtraction (TDCS), as previously validated (Meikle et al., 1994; Narita et al., 1996; Iida et al., 1998). The TDCS can provide the pixel-by-pixel estimation, $k(x, y)$, of scatter component in measured emission data, by means of the following formulation:

$$k(x,y) = 1 - \frac{1}{A - B \cdot t(x,y)^{\beta/2}} + k_0 \tag{4}$$

where $t(x, y)$ is an attenuation factor for pixel (x, y) and k_0 is a term illustrating both septal penetration and scatter in the collimator due to contamination of high-energy photon of ^{123}I. The parameter sets for TDCS are $A=2.4718$, $B=A-1$, $\beta=0.2088$, and $k_0=0.2141$ for the triple-headed camera, $A=2.3069$, $B=A-1$, $\beta=0.2926$, and $k_0=0.3000$ for the dual-headed camera, respectively. These parameters were empirically determined by the previous study (Kim et al., 2001). The scatter-corrected projections were then reconstructed using the in-house package for quantitative SPECT reconstruction (QSPECT), which employed the ordered-subset expectation maximization (OS-EM) algorithm including the attenuation correction with the attenuation map (Hudson and Larkin, 1994). The reconstructed images were then cross-calibrated to the well counter system using the cross-calibration factor determined as below.

Images of the cylindrical phantom were reconstructed following the same procedures as for the clinical study, including correction for scatter and attenuation. A circular region-of-interest (ROI) of 8-cm diameter was placed on the transverse image, and mean counts over this ROI were referred to the radioactivity concentration of this solution (cps/g) measured by the well counter. The ratio of these two values was defined as the cross-calibration factor between the SPECT and the well counter system.

Data analysis

The reconstructed images of the first and second session were realigned using SPM2, to correct a possible head motion between both scan sessions. Quantitative CBF images were calculated for both the first and second SPECT images, respectively, as described in the theory, with setting T^{bkg} to T_1. The distribution volume of IMP, V_d, was fixed at 35 ml/ml in the CBF calculation (Hatazawa et al., 1997; Iida et al., 1998). The image of background radioactivity generated during CBF calculation was compared with the reconstructed image immediately before the second IMP injection, i.e., the image with scan duration of 20–30 min for the first and second groups, and 20–25 min for the third group, respectively. All calculated CBF images of SPECT and PET were co-registered to its own MRI image, using SPM2.

In total, 39 circular ROIs with 2 cm of diameter were placed on MRI image, to cover the whole brain according to the criteria described elsewhere (Yamaguchi et al., 1986; Iida et al., 1998). These ROIs were projected on all CBF images to investigate the reproducibility between the first and second scans, and the consistency of the proposed method with PET. The rest–rest study was used to evaluate the reproducibility of the estimated CBF values between the two sessions, while the rest–acetazolamide study was used to evaluate the vasareactivity in normal subjects (namely the second group). Consistency of the calculated CBF values between the present method and PET was also evaluated.

All data were presented as mean ± SD, and Pearson's correlation and linear regression analysis were used to evaluate relationships between the two CBF values. The reproducibility of both measured and estimated background images was evaluated by means of Mann–Whitney rank sum test.

Results

Figs. 3A–C show a comparison of the background radioactivity concentration at 25 min after the first IMP injection estimated by the present model-based approach, with those obtained from a scan with short duration. Fig. 3A is a typical comparison of the background images obtained from one study among the first group. It appears that the estimated images show visually smoother, therefore smaller noise, than the measured images, while the absolute counts are equivalent. ROI counts of the estimated background images were also compared with those of the measured images for the rest–rest studies of the 1st group and the rest–acetazolamide studies of the third group in Figs. 3B and C, respectively. There is no significant difference between the two methods both in the rest–rest ($p>0.5$) and rest–acetazolamide ($p>0.1$) studies. However, the rest–acetazolamide study indicated slightly greater spread about the regression line.

Fig. 4A shows comparison of CBF images obtained from one of the rest–rest studies, indicating the reproducibility of the CBF measurement by the present method (Dual-Table ARG method). The visual difference between the estimated and measured background images in Fig. 3A leaded to the similar quality between the first and second CBF image set, although there is some difference in noise between test and retest. It is clear that the quantitative values of CBF are consistent between the two CBF images obtained from the first and second scans (see also Fig. 4B). The reproducibility between the two CBF values obtained from the rest–rest study as evaluated as a deviation of the two averages between the first and second CBF values was 1.5±5.7%. There was no significant difference between them.

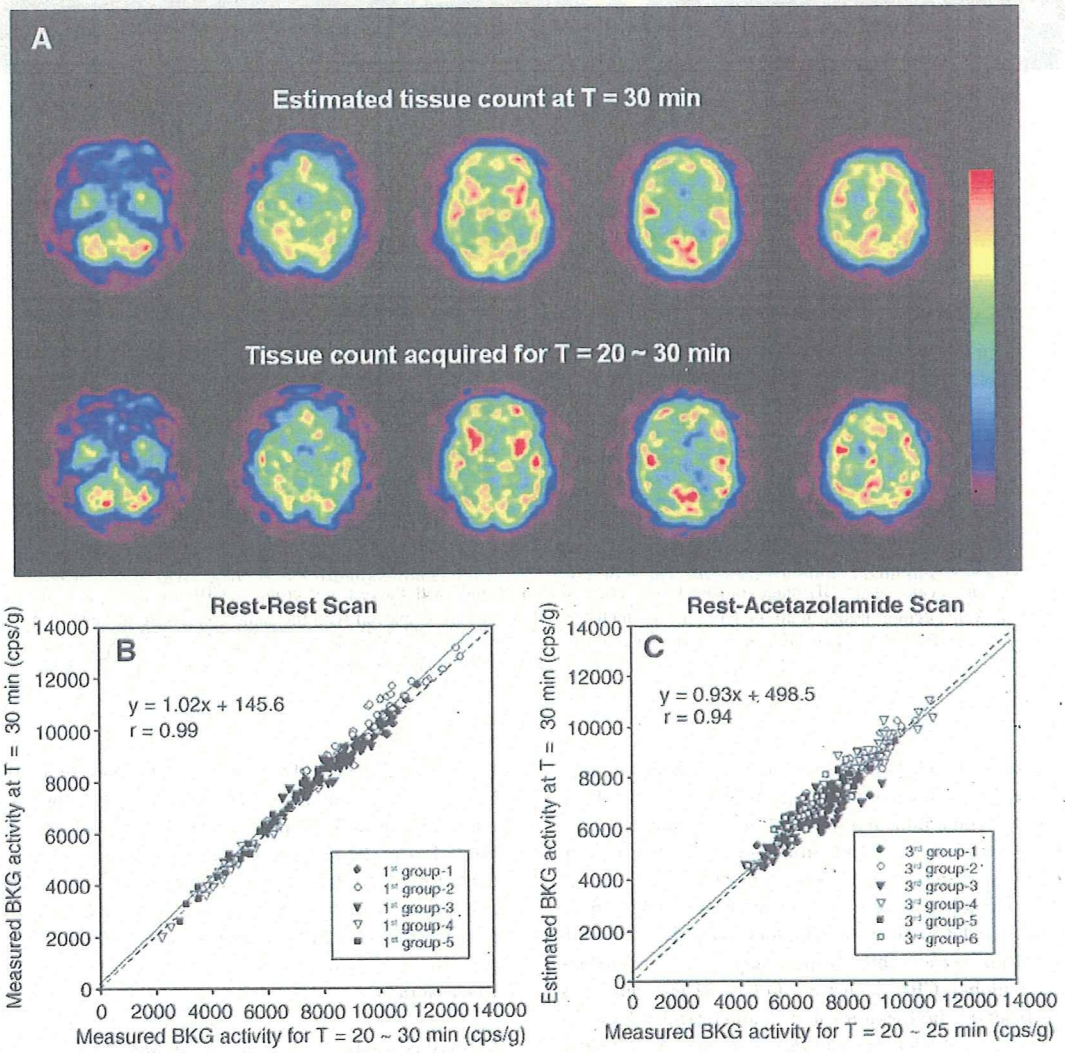

Fig. 3. (A) Comparison of background images estimated by the proposed method (top) with those acquired by a 10-min scan (t=20–30 min) with the triple-headed camera. (B) Comparison of pixel counts estimated by the proposed method with those acquired by a 10-min scan with the triple-headed camera. Values were obtained from 39 circular regions of interest that had a size of 314 mm^2. Data are obtained from the rest–rest studies (n=5), and regression lines are plotted for each subject. (C) Same as for panel (B) but from the rest–acetazolamide studies, in which background activity was compared with those by a 5-min scan (t=20–25 min) with dual-headed camera.

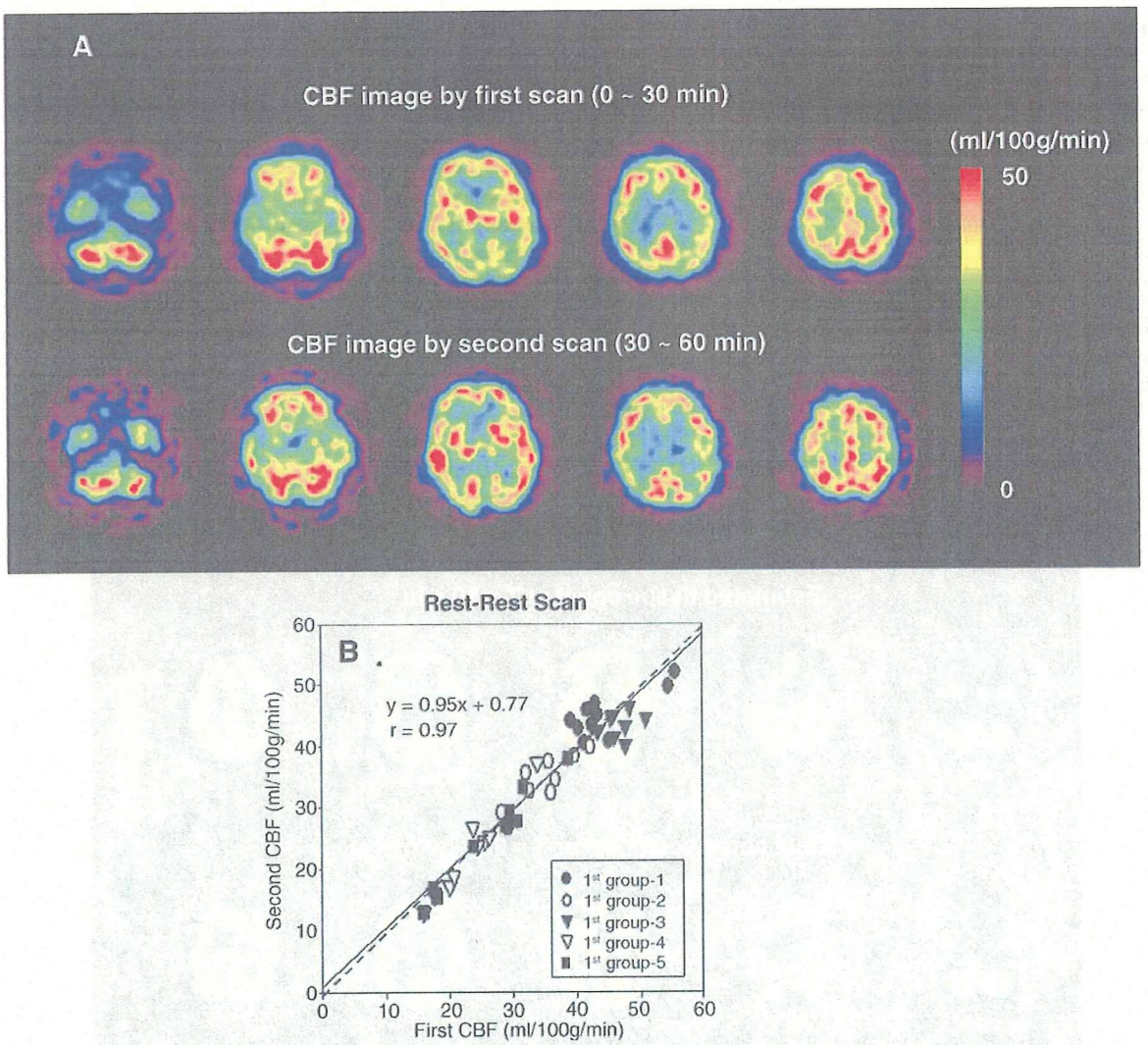

Fig. 4. (A) A comparison of calculated CBF images obtained from a typical clinical study with the rest–rest protocol. CBF images are shown for both first (top) and second (bottom) scans, demonstrating reproducibility of the method. All images are displayed with the same color scale in units of ml/100 g/min. (B) Comparison of calculated CBF values obtained from the rest–rest studies ($n=5$). Each value corresponds to a mean value of regions of interest in each area of deep and cortical gray matter (frontal, temporal, occipital gyri) and cerebellum. No significant difference was observed between the first and the second CBF values.

In the second group, CBF values of three gray matter regions (e.g., cortical and deep gray matter and cerebellum) were 37.4 ml/100 g/min, 36.4 ml/100 g/min, and 44.4 ml/100 g/min for rest state, and 53.1 ml/100 g/min, 51.5 ml/100 g/min, and 63.7 ml/100 g/min for acetazolamide state, respectively (Figs. 5A, B). The CBF values of whole region including white matter, which were obtained from the 39 ROIs, were 37.1±5.0 ml/100 g/min for rest and 52.2±8.0 ml/100 g/min for acetazolamide states, respectively. These CBF values resulted in the global CBF increase of 40.5±9.4%, and was homogeneous in all cerebral regions (43.0% for cortical, 42.3% for deep gray matter and 39.4% cerebellum). This increase of 40% agreed with the literature value (Hayashida et al., 1996). No significant difference in the amount of increase was observed among the regions (see Fig. 5B).

Figs. 6A–C show the results of comparison of rest–acetazolamide studies with SPECT and PET. The CBF images by both the Dual-Table ARG SPECT and $H_2^{15}O$ ARG PET methods were similar both quantitatively and qualitatively (Fig. 6A). The CBF values by the SPECT method showed the consistency with those by PET over the regions of deep and cortical gray matter (frontal, temporal, occipital gyri) and cerebellum (Fig. 6B), and this consistency resulted in the good correlation of CBF increase between PET and SPECT (Fig. 6C).

Discussion

In this study, we developed a new method of quantitative CBF mapping, which is based on the mathematical formulation for repeat CBF quantitation using a diffusible tracer that incorporates time-dependent changes of tissue radioactivity distribution, and showed that this method allows the test–retest assessment of quantitative CBF images within a reasonable scan

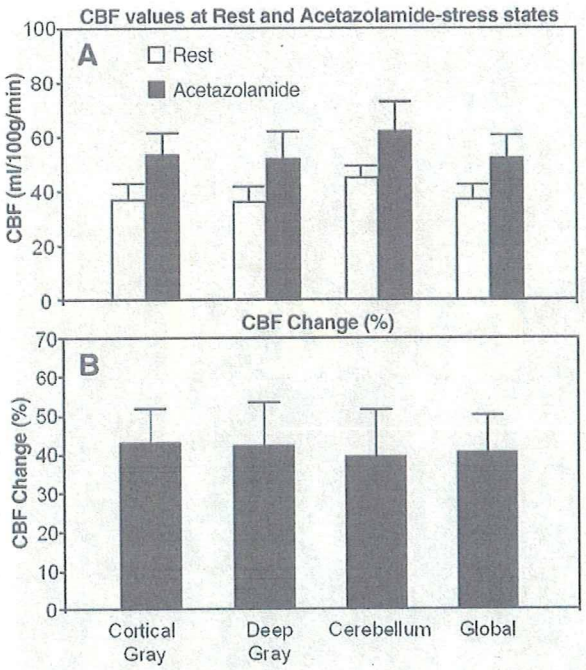

Fig. 5. (A) CBF values at both of rest and acetazolamide-stress states and (B) %change of CBF obtained from the rest–acetazolamide studies performed on the second group. The values of CBF and %change of three gray matter regions, namely the cortical and deep gray matter and cerebellum, and the whole brain regions, were summarized. No significant difference was observed in the %change among the regions.

interval. The noise enhancement, which has been a major restriction in previous approaches when using a simplified background subtraction technique, has been suppressed with the present approach.

Validity of this method has been demonstrated in sequential SPECT studies at rest and after acetazolamide in conjunction with a split-dose administration of IMP. IMP is a diffusible tracer with significant clearance from the brain over time (Kuhl et al., 1982; Iida et al., 1994a,b). It should, however, be noted that the kinetic behavior of IMP can be well described by a mathematical model (single-tissue compartment model). Thus, in this study, the formulation was given, based on the single-tissue compartment model, for a split-dose administration protocol, allowing the accurate quantitation of CBF at two physiological conditions. The quantitative accuracy and the precision of this approach at rest and after acetazolamide are acceptable in the clinical setting, allowing the rest–acetazolamide study to be carried out with a total study time of less than 1 h with an interval of 20 to 30 min between the two IMP administrations.

The new formulation that estimates the second CBF from the second SPECT scan by incorporating the background radioactivity from the previous scan into the formulation, has been validated successfully in this study with clinical scans. The calculated CBF images were consistent between the first and the second scans in the rest–rest study, in which image quality of the second CBF was not different from that from the first scan. In the previous work (Iida et al., 2000), we have evaluated the reproducibility of both CBF image in rest–rest study, using 160 square ROIs (34×34 mm^2) those were placed on brain region including gray and white matter of 5 tomographic slices of CBF images at axial position shown in Figs. 3A and 4A, and obtained the difference within 3%. In other study presented in domestic meeting (Annual meeting of Japanese Society of Nuclear Medicine (2000)), we have also compared the test–retest CBF image sets generated in rest–rest study by the presented method, with those by a traditional microsphere method (Kuhl et al., 1982), and found same reproducibility of the both test–retest CBF images for the both CBF calculation methods, with better quality of the second CBF image by the presented method than by the traditional method. Therefore, from these previous results showing enough accuracy of reproducibility over whole brain regions, we have focused the variation of CBF values in regions those have been interested in many clinical studies, rather than whole brain regions. The rest–acetazolamide study also demonstrated reasonable quality of CBF images both at rest and after acetazolamide. The estimated values of CBF at both rest and acetazolamide states, and %increase of CBF showed a good linear relationship with those by $H_2^{15}O$ PET, although there was a small offset in the comparison of %increase of CBF. This small bias was resulted from the slight underestimation of background radioactivity, which might be affected by reconstructed image with lower count statistics due to the fewer number of detector and relatively higher scatter fraction in the data acquired from dual-headed camera, compared to that of triple-headed camera (k_0=0.3000 for dual-headed and k_0=0.2141 for triple-headed). The amount of about 40% increase of CBF in healthy volunteers, however, agreed with the literature values, which also suggests validity of the present method (Hayashida et al., 1996).

The transient distribution of the tissue radioactivity concentration at the time of the second IMP injection can be accurately estimated from the first scan with the present method with minimal enhancement of statistical noise. It was shown that this estimated tissue radioactivity distribution was in a good agreement with that directly measured by a short (10 min or 5 min) SPECT scan, without enhancement of statistical noise (Fig. 3A). It is important to note that this agreement was confirmed not only in the rest–rest protocol (Fig. 3B), but also in the rest–acetazolamide protocol (Fig. 3C), in which the acetazolamide challenge was given during the 1st SPECT scan. This can be understood by referring to the approximate formulation of the transient contribution weight as defined in Eq. (3). As has been described in theory, the transient contribution is approximately proportional to the first-derivative of the tissue radioactivity concentration, and thus highly weighted only at the early phase after the tracer administration, but small after the peak of tissue radioactivity when a bolus administration protocol in employed. CBF changes some time after the immediate period post IMP injection have only a very small or negligible effect on the background activity. Eq. (2) also implies that the estimated CBF maps at rest and after acetazolamide are highly weighted to the early period immediately after each of IMP administrations, which has been shown in the previous study using simulation (Iida et al., 2000). From these findings, it can be expected that the second CBF should yield the elevated CBF values even though CBF is decreased after a certain period such as >10 min after the 2nd IMP administration.

In general, kinetic analysis in PET or SPECT assumes a constant physiological condition throughout the whole study period, and only a single set of physiological parameters such as CBF is typically estimated from a series of data. The temporal resolution of the PET/SPECT methodology has therefore been

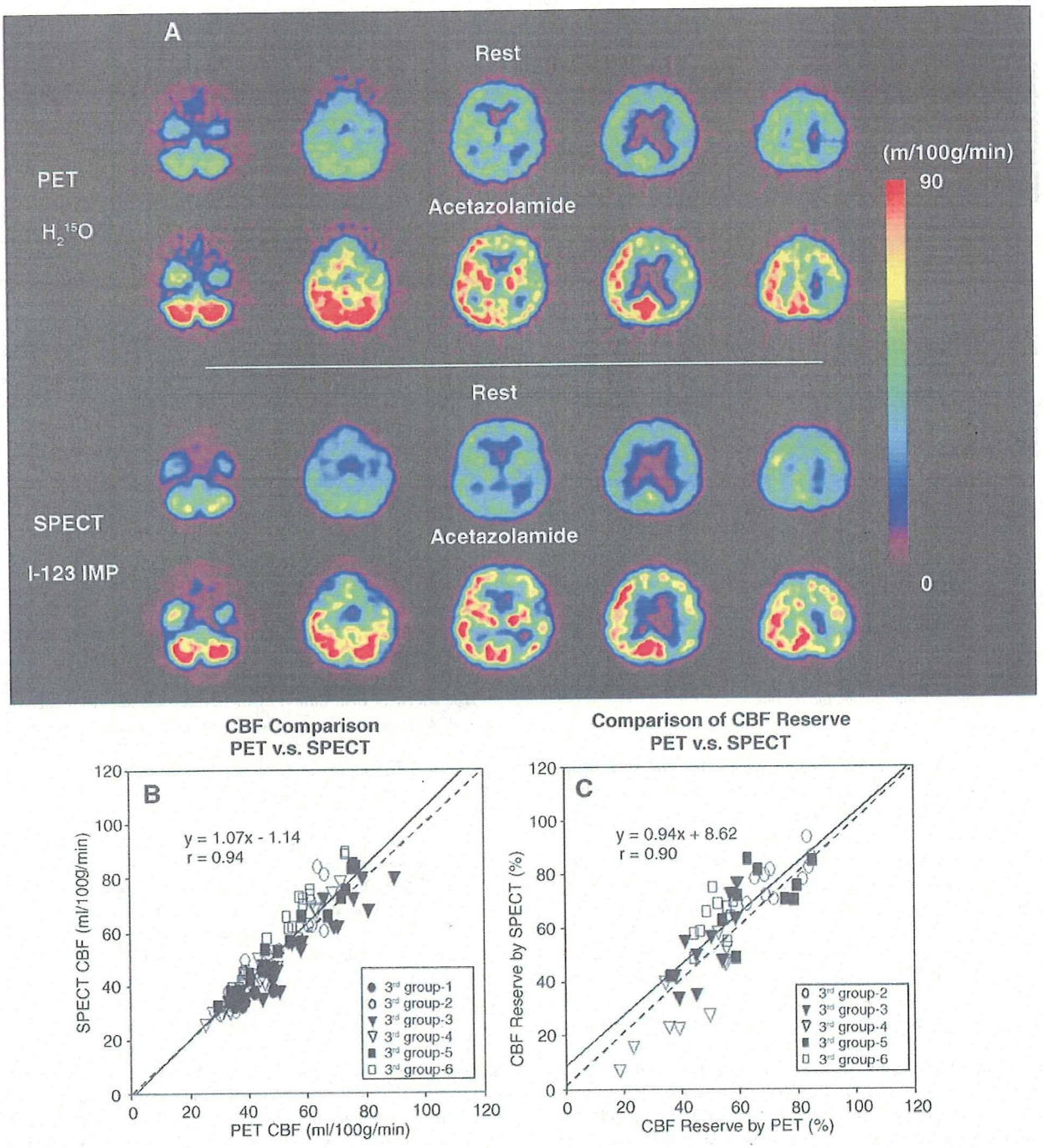

Fig. 6. (A) A comparison of calculated CBF images obtained by PET (top two) and SPECT (bottom two) from a typical clinical study with the rest–acetazolamide protocol. CBF images are shown for both first (first and third rows) and second (second and forth images) scans, respectively, and reveal that the present method is comparable with that by PET in CBF estimation. CBF images obtained by the present method (bottom two) were also compared with those (top two) by the conventional $H_2^{15}O$ ARG PET. All images are displayed with the same color scale in units of ml/100 g/min. (B) Comparison of calculated CBF values obtained from the rest–acetazolamide studies with dual-headed camera and PET (n=6). Each value corresponds to a mean value of regions of interest in each area of deep and cortical gray matter (frontal, temporal, occipital gyri) and cerebellum. (C) Comparison of %increase of CBF values calculated with the CBF values of (B). %Increase of CBF was calculated by ([CBF(acetazolamide)/CBF(rest)] − 1) × 100.

restricted by this limitation. It is, however, important to note that the CBF estimated by the present method was highly weighted by the transient CBF for a certain period. This contribution of transient weight in the estimated CBF has been discussed already in previous publications for $H_2^{15}O$ PET ARG (Iida et al., 1991), and this has been applied to cognitive activation studies to detect 30-s

momentary change (Silbersweig et al., 1993, 1994). All of these findings support the validity of the present Dual-Table ARG approach for estimating CBF maps with the split-dose administration of IMP.

The evaluation of rest–acetazolamide CBF was a goal of the application of this methodology. This is based on the on-going project in Japan, which re-evaluates the previous reports regarding the value of extracranial/intracranial arterial anastomosis in patients with symptomatic occlusive disease of the internal carotid artery (Vortrup et al., 1984; The-EC/IC-Bypass-Study-Group, 1985a,b; Vortrup et al., 1986). The previous study failed to show significant efficacy of the bypass surgery, but it did not selected patients by the aid of information for cerebral hemodynamics using functional imaging. The on-going project is intended to select only the severely ischemic patients (Stage II ischemia) by means of evaluating the reduced baseline CBF with a lack of vasareactivity after acetazolamide challenge (Powers, 1991; Hayashida et al., 1996, 1999). PET is able to provide useful information (Powers and Raichle, 1985), but due to its limited availability in clinical centers, this Dual-Table ARG approach with IMP and SPECT may be of use for this project. A further evaluation is needed to confirm this.

The present Dual-Table ARG method may be applied to other tracer studies. Chmielowska et al. (1998, 1999) claimed that the qualitative CBF mapping during cognitive activation may be obtained with a 6-min interval by involving a simple background subtraction, yielding consistent activation foci as compared with a traditional protocol based on repeat PET scanning with repeat $H_2^{15}O$ injection at 10- to 12-min interval. DT-ARG approach to various tracer studies was evaluated by simulation (Iida et al., 2000), in which dual bolus administration and transient CBF change were simulated with assumption of V_d=28 for IMP and V_d=0.8 for $H_2^{15}O$, respectively. The simulation demonstrated that the increased CBF is estimated only when the true CBF was increase at the extremely early phase after the administration of IMP or $H_2^{15}O$, while the second CBF was independent of the change of CBF during previous scans in the both IMP and $H_2^{15}O$ simulations. Application of the present Dual-Table ARG approach to the $H_2^{15}O$ PET activation study may be able to further shorten the scan interval (approximately 1.5 min) (Watabe et al., 2002), by incorporating the background radioactivity distribution into the kinetic model formulation. Another possibility is the quantitative $CMRO_2$ study by means of PET scans following sequential administration of $^{15}O_2$ and $H_2^{15}O$. The previous protocol proposed by Mintun et al. (1984) was based on independent three step measurements following each of the $C^{15}O$, $^{15}O_2$ and $H_2^{15}O$ administration. The present approach, with the help of the estimated background radioactivity distribution in the sequential administration, could reduce the intervals between the scans without the loss of quantitative accuracy and image quality of each functional images of $CMRO_2$ and CBF, respectively, in anesthetized monkey study (Kudomi et al., 2005). Systematic studies are obviously needed in order to evaluate the feasibility of this technique in clinical studies.

We have previously demonstrated the importance of accurate image reconstruction in SPECT and employed a novel program package in order to achieve accurate reconstruction. Scatter, which was shown to cause serious reduction of the image contrast between the high CBF and low CBF areas, was corrected by the previously validated TDCS method (Meikle et al., 1994; Narita et al., 1996; Iida et al., 1998) together with correction for the penetration from the high-energy contamination (Kim et al., 2001). The photon attenuation correction was included in the OS-EM reconstruction procedure by using the attenuation map that was estimated from the head contour of its own MRI image (Iida et al., 1998). Details of the procedures and their validation have been described elsewhere (Iida et al., 1998; Kim et al., 2001). These procedures improved image contrast, and enabled to provide quantitative image that are equivalent to PET (y(ml/100 g/min)=1.07× (ml/100 g/min)−1.14, r=0.94).

In conclusion, CBF can be quantified by means of split-dose administration of IMP using SPECT. Contribution of the background radioactivity attributed to the previous administration of radiotracer can be built into the model, with minimal enhancement of statistical noise. The estimated CBF appeared to be most sensitive to the transient CBF immediately after the IMP injection but not to later periods, thus allowing the pharmacological challenges even during the first SPECT scan. Repeat quantitation of CBF could be feasible with considerably shorter intervals than with previous approaches. Accuracy of this approach was sufficiently high and may be of use for clinical studies.

Acknowledgment

This study was supported by the Program for Promotion of Fundamental Studies in Health Science of the Organization for Pharmaceutical Safety and Research (of Japan).

References

Chmielowska, J., Coghill, R.C., Maisog, J.M., Carson, R.E., Herscovitch, P., Honda, M., Chen, R., Hallett, M., 1998. Positron emission tomography [^{15}O]water studies with short interscan interval for single-subject and group analysis: influence of background subtraction. J. Cereb. Blood Flow Metab. 18, 433–443.

Chmielowska, J., Coghill, R.C., Carson, R.E., Ishii, K., Chen, R., Hallett, M., Herscovitch, P., 1999. Comparison of PET [^{15}O] water studies with 6-minute and 10-minute interscan intervals: single-subject and group analyses. J. Cereb. Blood Flow Metab. 19, 570–582.

Hashikawa, K., Matsumoto, M., Moriwaki, H., Oku, N., Okazaki, Y., Uehara, T., Handa, N., Kusuoka, H., Kamada, T., Nishimura, T., 1994. Split dose iodine-123-IMP SPECT: sequential quantitative regional cerebral blood flow change with pharmacological intervention. J. Nucl. Med. 35, 1226–1233.

Hatazawa, J., Iida, H., Shimosegawa, E., Sato, T., Murakami, M., Miura, Y., 1997. Regional cerebral blood flow measurement with iodine-123-IMP autoradiography: normal values, reproducibility and sensitivity to hypoperfusion. J. Nucl. Med. 38, 1102–1108.

Hattori, N., Yonekura, Y., Tanaka, F., Fujita, T., Wang, J., Ishizu, K., Okazawa, H., Tamaki, N., Konishi, J., 1996. One-day protocol for cerebral perfusion reserve with acetazolamide. J. Nucl. Med. 37, 2057–2061.

Hayashida, K., Tanaka, Y., Hirose, Y., Kume, N., Iwama, T., Miyake, Y., Ishida, Y., Matsuura, H., Miyake, Y., Nishimura, T., 1996. Vasoreactive effect of acetazolamide as a function of time with sequential PET ^{15}O-water measurement. Nucl. Med. Commun. 17, 1047–1051.

Hayashida, K., Fukuchi, K., Hasegawa, Y., Kume, N., Cho, I.H., Nishimura, T., 1999. Viable tissue in an area of severely reduced perfusion demonstrated with I-123 iomazenil brain SPECT imaging of benzodiazepine receptors. Clin. Nucl. Med. 24, 576–578.

Hudson, H.M., Larkin, R.S., 1994. Accelerated image reconstruction using ordered subsets of projection data. IEEE Trans. Med. Imaging 13, 601–609.

Iida, H., Kanno, I., Miura, S., Murakami, M., Takahashi, K., Uemura, K., 1986. Error analysis of a quantitative cerebral blood flow measurement using $H_2^{15}O$ autoradiography and positron emission tomography, with respect to the dispersion of the input function. J. Cereb. Blood Flow Metab. 6, 536–545.

Iida, H., Higano, S., Tomura, N., Shishido, F., Kanno, I., Miura, S., Murakami, M., Takahashi, K., Sasaki, H., Uemura, K., 1988. Evaluation of regional differences of tracer appearance time in cerebral tissues using [^{15}O] water and dynamic positron emission tomography. J. Cereb. Blood Flow Metab. 8, 285–288.

Iida, H., Kanno, I., Miura, S., Murakami, M., Takahashi, K., Uemura, K., 1989. A determination of the regional brain/blood partition coefficient of water using dynamic positron emission tomography. J. Cereb. Blood Flow Metab. 9, 874–885.

Iida, H., Kanno, I., Miura, S. (Eds.), 1991. Rapid Measurement of Cerebral Blood Flow with Positron Emission Tomography. Exploring the Brain Functional Anatomy with Positron Tomography. John Wiley & Sons, Chichester.

Iida, H., Itoh, H., Bloomfield, P.M., Munaka, M., Higano, S., Murakami, M., Inugami, A., Eberl, S., Aizawa, Y., Kanno, I., Uemura, K., 1994a. A method to quantitate cerebral blood flow using a rotating gamma camera and iodine-123 iodoamphetamine with one blood sampling. Eur J. Nucl. Med. Mol. Imaging 21, 1072–1084.

Iida, H., Itoh, H., Nakazawa, M., Hatazawa, J., Nishimura, H., Onishi, Y., Uemura, K., 1994b. Quantitative mapping of regional cerebral blood flow using iodine-123-IMP and SPECT. J. Nucl. Med. 35, 2019–2030.

Iida, H., Akutsu, T., Endo, K., Fukuda, H., Inoue, T., Ito, H., Koga, S., Komatani, A., Kuwabara, Y., Momose, T., Nishizawa, S., Odano, I., Ohkubo, M., Sasaki, Y., Suzuki, H., Tanada, S., Toyama, H., Yonekura, Y., Yoshida, T., Uemura, K., 1996. A multicenter validation of regional cerebral blood flow quantitation using [^{123}I]iodoamphetamine and single photon emission computed tomography. J. Cereb. Blood Flow Metab. 16, 781–793.

Iida, H., Narita, Y., Kado, H., Kashikura, A., Sugawara, S., Shoji, Y., Kinoshita, T., Ogawa, T., Eberl, S., 1998. Effects of scatter and attenuation correction on quantitative assessment of regional cerebral blood flow with SPECT. J. Nucl. Med. 39, 181–189.

Iida, H., Watabe, H., Shidahara, M., Kim, K.M., Ogura, T., 2000. Modeling strategy for background compensation in repeat cerebral blood flow quantitation with diffusible tracers. IEEE Med. Img. Conf. Proc. 2, 34–39.

Imaizumi, M., Kitagawa, K., Hashikawa, K., Oku, N., Teratani, T., Takasawa, M., Yoshikawa, T., Rishu, P., Ohtsuki, T., Hori, M., Matsumoto, M., Nishimura, T., 2002. Detection of misery perfusion with split-dose 123I-iodoamphetamine single-photon emission computed tomography in patients with carotid occlusive diseases. Stroke 33, 2217–2223.

Kanno, I., Iida, H., Miura, S., Murakami, M., Takahashi, K., Sasaki, H., Inugami, A., Shishido, F., Uemura, K., 1987. A system for cerebral blood flow measurement using an $H_2^{15}O$ autoradiographic method and positron emission tomography. J. Cereb. Blood Flow Metab. 7, 143–153.

Kim, K.M., Watabe, H., Shidahara, M., Ishida, Y., Iida, H., 2001. SPECT collimator dependency of scatter and validation of transmission dependent scatter compensation methodologies. IEEE Trans. Nucl. Sci. 48, 689–696.

Kudomi, N., Hayashi, T., Teramoto, N., Watabe, H., Kawachi, N., Ohta, Y., Kim, K.M., Iida, H., 2005. Rapid quantitative measurement of $CMRO_2$ and CBF with the dual administration of ^{15}O-labeled oxygen and water during a single PET scan—A validation study with error analysis in anesthetized monkeys. J. Cereb. Blood Flow Metab. 25, 1209–1224.

Kuhl, D.E., Barrio, J.R., Huang, S.C., Selin, C., Ackermann, R.F., Lear, J.L., Wu, J.L., Lin, T.H., Phelps, M.E., 1982. Quantifying local cerebral blood flow by *N*-isopropyl-*p*-[^{123}I]iodoamphetamine (IMP) tomography. J. Nucl. Med. 23, 196–203.

Kurisu, R., Ogura, T., Takikawa, S., Saito, H., Nakazawa, M., Iida, H., 2002. Estimation and optimization of the use of standard arterial input function for split-dose administration of *N*-isopropyl-*p*[^{123}I]iodoamphetamine. Kaku Igaku 39, 13–20.

Lear, J.L., Ackermann, R.F., Kameyama, M., Kuhl, D.E., 1982. Evaluation of [^{123}I]isopropyliodoamphetamine as a tracer for local cerebral blood flow using direct autoradiographic comparison. J. Cereb. Blood Flow Metab. 2, 179–185.

Meikle, S.R., Hutton, B.F., Bailey, D.L., 1994. A transmission-dependent method for scatter correction in SPECT. J. Nucl. Med. 35, 360–367.

Mintun, M.A., Raichle, M.E., Martin, W.R., Herscovitch, P., 1984. Brain oxygen utilization measured with O-15 radiotracers and positron emission tomography. J. Nucl. Med. 25, 177–187.

Narita, Y., Eberl, S., Iida, H., Hutton, B.F., Braun, M., Nakamura, T., Bautovich, G., 1996. Monte Carlo and experimental evaluation of accuracy and noise properties of two scatter correction methods for SPECT. Phys. Med. Biol. 41, 2481–2496.

Nishizawa, S., Iida, H., Tsuchida, T., Ito, H., Konishi, J., Yonekura, Y., 2003. Validation of the Dual-Table autoradiographic method to quantify two sequential rCBFs in a single SPET session with *N*-isopropyl-[^{123}I] *p*-iodoamphetamine. Eur J. Nucl. Med. Mol. Imaging 30, 943–950.

Oku, N., Matsumoto, M., Hashikawa, K., Moriwaki, H., Okazaki, Y., Seike, Y., Handa, N., Uchara, T., Kamada, T., Nishimura, T., 1994. Carbon dioxide reactivity by consecutive technetium-99m-HMPAO SPECT in patients with a chronically obstructed major cerebral artery. J. Nucl. Med. 35 (1), 32–40.

Powers, W.J., 1991. Cerebral hemodynamics in ischemic cerebrovascular disease. Ann. Neurol. 29, 231–240.

Powers, W.J., Raichle, M.E., 1985. Positron emission tomography and its application to the study of cerebrovascular disease in man. Stroke 16, 361–376.

Silbersweig, D.A., Stern, E., Frith, C.D., Cahill, C., Schnorr, L., Grootoonk, S., Spinks, T., Clark, J., Frackowiak, R., Jones, T., 1993. Detection of thirty-second cognitive activations in single subjects with positron emission tomography: a new low-dose $H_2^{15}O$ regional cerebral blood flow three-dimensional imaging technique. J. Cereb. Blood Flow Metab. 13, 617–629.

Silbersweig, D.A., Stern, E., Schnorr, L., Frith, C.D., Ashburner, J., Cahill, C., Frackowiak, R.S., Jones, T., 1994. Imaging transient, randomly occurring neuropsychological events in single subjects with positron emission tomography: an event-related count rate correlational analysis. J. Cereb. Blood Flow Metab. 14, 771–782.

The-EC/IC-Bypass-Study-Group, 1985a. Failure of extracranial–intracranial arterial bypass to reduce the risk of ischemic stroke. Results of an international randomized trial. N. Engl. J. Med. 313, 1191–1200.

The-EC/IC-Bypass-Study-Group, 1985b. The international cooperative study of extracranial/intracranial arterial anastomosis (EC/IC bypass study): methodology and entry characteristics. Stroke 16, 397–406.

Vortrup, S., Henriksen, L., Paulson, O.B., 1984. Effect of acetazolamide on cerebral blood flow and cerebral metabolic rate of oxygen. J. Clin. Invest. 74, 1634–1639.

Vortrup, S., Brun, B., Lassen, N.A., 1986. Evaluation of the cerebral vasodilatory capacity by the acetazolamide test before EC-IC bypass surgery in patients with occlusion of the internal carotid artery. Stroke 17, 1291–1298.

Watabe, H., Kondoh, Y., Kim, K.M., Shidahara, M., Iida, H. (Eds.), 2002. Shortening rCBF Measurement Interval in [^{15}O]H2O PET. Brain Imaging Using PET. Academic Press, San Diego.

Yamaguchi, T., Kanno, I., Uemura, K., Shishido, F., Inugami, A., Ogawa, T., Murakami, M., Suzuki, K., 1986. Reduction in regional cerebral metabolic rate of oxygen during human aging. Stroke 17, 1220–1228.

ORIGINAL ARTICLE

Annals of Nuclear Medicine Vol. 20, No. 9, 605–613, 2006

Predicting human performance by channelized Hotelling observer in discriminating between Alzheimer's dementia and controls using statistically processed brain perfusion SPECT

Miho SHIDAHARA,* Kentaro INOUE,* Masahiro MARUYAMA,** Hiroshi WATABE,*** Yasuyuki TAKI,* Ryoi GOTO,* Ken OKADA,* Shigeo KINOMURA,* Shinichiro OSAWA,* Yoshimi ONISHI,**** Hiroshi ITO,* Hiroyuki ARAI***** and Hiroshi FUKUDA*

*Department of Radiology and Nuclear Medicine, Institute of Development, Aging and Cancer, Tohoku University
**Department of Geriatric and Respiratory Medicine, Tohoku University School of Medicine
***Department of Investigative Radiology, National Cardio-vascular Center Research Institute
****Section for Medical Image Information Systems, Research Center for Frontier Medical Engineering, Chiba University
*****Department of Geriatric and Complementary Medicine, Center for Asian Traditional Medicine Research, Tohoku University School of Medicine

Objective: We compared the diagnostic accuracy achieved by a human observer (nuclear medicine physician) and a channelized Hotelling (CH) observer on the basis of receiver-operating characteristics (ROC) curve for the differential diagnosis of Alzheimer's disease (AD) from SPECT images. ***Methods:*** The I-123-IMP brain perfusion SPECT images of 42 subjects (21 AD patients and 21 healthy controls) were used for an interpretation study and those of 10 healthy subjects were for a normal database. SPECT images were processed into four types: original SPECT images, three-dimensional stereotactic surface projection (3DSSP) images derived from them, Z-scores of SPECT images, and Z-scores of 3DSSP images. Five nuclear medicine physicians evaluated the test dataset sequentially as to whether the presented images were those of AD patients, which were rated using five categories of certainty: definitely, possibly, equivocally, possibly not, and definitely not. The test statistics (λ) of the dataset generated by the CH observer were rated for ROC analysis. The areas under the ROC curves (Az) for the four image types interpreted by the human and CH observers were estimated and compared. ***Results:*** Among the four image types, the best performance based on Az obtained by both the CH and human observers was observed for the Z-score of 3DSSP images, and the lowest was for the original SPECT images. ***Conclusions:*** The performance of the CH observer was similar to that of the human observers, and both were dependent on the image type. This indicates that the CH observer may predict human performance in discriminating Alzheimer's dementia and can be useful for comparing and optimizing image processing methods of brain perfusion SPECT without human observers.

Key words: channelized Hotelling observer, Alzheimer's disease, single-photon emission tomography, ROC analysis, three-dimensional stereotactic surface projection

INTRODUCTION

RECENTLY, new medications such as cholinesterase inhibitors have been reported to effectively delay Alzheimer's disease (AD) progression.[1] This finding has increased the importance of an early diagnosis of AD. Thus, over the past several years, much effort has been made to detect AD and to improve the detection of AD on interpretation of brain perfusion SPECT.[2–12] For instance,

Received May 22, 2006, revision accepted August 29, 2006.
For reprint contact: Miho Shidahara, Ph.D., Department of Radiology and Nuclear Medicine, Institute of Development, Aging and Cancer, Tohoku University, Seiryou-machi 4–1, Aoba-ku, Sendai, Miyagi 980–8575, JAPAN.
E-mail: sidahara@idac.tohoku.ac.jp